ISSN: 2472-3703 DOI: 10.6911/WSRJ.202212_8(12).0020

Calculation Method of Crack Stiffness of Gear Body Based on Potential Energy Method

Zhiwen Xuan[1, a, *], Fuhao Liu[1], Yaobing Li[1], Shen Guo[1], Chao Ye[1], Huailiang Su[1]

[1] School of Mechanical and Automotive Engineering, Qingdao University of Technology, Qingdao, Shandong, 266525, China

[a] Corresponding author E-mail: zhiwen_xuan_sdust@163.com

Abstract

In the conventional meshing stiffness calculation model, it is usually assumed that the root crack exists only in the root portion of the tooth. However, during the meshing process, the root crack extends under the meshing force, and when the root crack extends into the base part of the gear, the meshing stiffness of the cracked tooth and the dynamic response of the gear system are different from the case when the crack exists only in the root part. Little research has been done to investigate the effect of the root crack on the meshing stiffness and dynamic response when the crack extends into the gear matrix. Therefore, an improved model for calculating the mesh stiffness of cracked gears is proposed in this paper, in which the gear base stiffness and gear tooth stiffness are calculated separately when the root crack is considered to extend into the gear base. Then, the accuracy of the proposed model is verified by the finite element method (FEM).

Keywords

Time-varying mesh stiffness; Gear body crack; Gear body stiffness; Gear tooth stiffness.

1. INTRODUCTION

Gears are an important basic component of mechanical equipment. Most major types of mechanical equipment are driven by gears. In gearing, the meshing stiffness is the main dynamic excitation in the gear meshing process. However, the structure of the gear train is becoming increasingly complex, the working environment is relatively harsh, and the gear train is prone to various failures throughout its life cycle. Among them, cracking is the most common failure mode. Therefore, it is very important to accurately calculate the meshing stiffness of gears containing cracks in order to accurately estimate the life of gears as well as for fault diagnosis.

Since the middle of the last century, analytical methods have received a lot of attention worldwide due to their high computational efficiency and acceptable agreement with finite element results in the calculation of gear mesh stiffness. As for analytical method, the most commonly used is the energy method. Weber[1], Cornell[2], Yang[3], Tian[4], Sainsot[5], and Shao et al.[6] finally determined the gear stiffness as the sum of five stiffnesses including gear body stiffness, compression stiffness, bending stiffness, shear stiffness, and Hertzian contact stiffness by continuously refining the energy method. The calculation of the stiffness of spur gears containing crack is basically done on the basis of the energy method. Wang et al.[7] analyzed the dynamics of tooth crack and obtained the mesh stiffness, load sharing performance and mesh characteristics. Chaari et al.[8] proposed the calculation model of gear tooth peeling and fracture, and studied the mesh stiffness and dynamic characteristics caused by gear failure. Chen et al.[6] studied the dynamic response of cracked spur gears and the

ISSN: 2472-3703 DOI: 10.6911/WSRJ.202212_8(12).0020

influence of crack depth, established the mesh stiffness calculation model of modified spur gears with tooth profile cracks, and proposed a non-uniform distribution along the tooth width. The analytical model of the mesh stiffness of the root crack is improved on the basis of the two-dimensional analytical formula proposed by Sainsot[5], and the influence of the root crack on the stiffness of the gear body can be calculated. Pandya and Parey[9] used PEM and variable crack intersection method to evaluate the total mesh stiffness, and proposed the cumulative reduction index to evaluate the influence of gear parameters on the mesh stiffness of cylindrical gear with cracks. Wan et al.[10] used the improved mesh stiffness to study the dynamic response of the gear-rotor coupling system when the gear crack appeared on the gear teeth. Ma et al.[11] studied the dynamic characteristics of gear-rotor system under the condition of tooth cracking. The time-varying mesh stiffness of CPT and CPR gears was obtained by FE method. The analytical formula for calculating the time-varying mesh stiffness of CPT gears was derived, and the dynamic response of gears under crack conditions was analyzed. Chen et al.[12] considered the reduction of wheel stiffness caused by the change of effective area between the tooth root circle and the rim circle, and proposed the calculation formula of CPR. Liang et al.[13] calculated the mesh stiffness of the cracked planet gear system.

Among the previous work, the changes of body stiffness caused by crack penetrating into the gear body were not considered. In this paper, energy method and analytical finite element method were combined to explore the effects of three different crack depths on the mesh stiffness of gear pairs.

2. THE IMPROVED MESH STIFFNESS CALCULATION MODEL OF GEAR

2.1. The exact tooth profile parametric equation considering the machining process

The proposed stiffness calculation model of the gear is shown in Figure 1. Considering the actual working condition of the gear, the gear is connected to the gear shaft by spline. Therefore, in this paper, the inner hole of the gear is fixed and the energy method in material mechanics is used to calculate the meshing stiffness of the gear. The fixed nodes are evenly distributed on the inner holes, n $(n = 2^{k+1}, k = 1,2,3 \ldots)$ represents the number of fixed nodes.

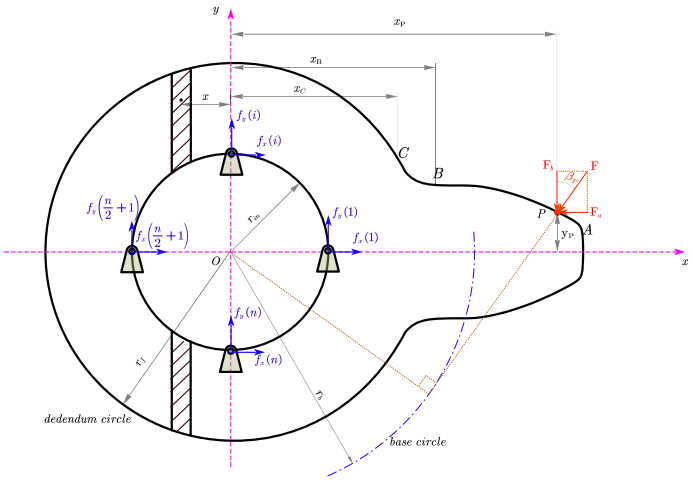

Figure 1. Model of a normal gear tooth

As showen on Figure 1. Rejoin tooth center line with Y axis. The DC segment represents the gear body, which are expressed as Eq.(1). Section CB is a dedendum transition curve, which are expressed as Eq.(2). Section BA is an involute curve, which are expressed as Eq.(3). Nodes fixed on the inner hole are numbered counterclockwise from the rightmost end of the

ISSN: 2472-3703 DOI: 10.6911/WSRJ.202212_8(12).0020

inner hole, the node at the right end is numbered 1, so number of the leftmost node is $n/2+1$. F_a and F_b are the two perpendicular component forces of the mesh force. x_P and y_P represent the x-coordinate and y-coordinate of the contact point P. x_B is the x-coordinate of the point B. x_C is the x-coordinate of the point C. x is the x-coordinate of the midpoint of any cross section. $f_x(i)$ stand for the horizontal support reaction of any fixed node, and $f_y(i)$ stand for the vertical support reaction of any fixed node. r_{in} indicates the radius of the shaft hole, r_b and r_f refer to the radius of the base and dedendum circle.

$$\begin{cases} x_1(\gamma) = r_f \cos(\gamma) \\ y_1(\gamma) = r_f \sin(\gamma) \end{cases} \tag{1}$$

Where γ represents the angle between the radial diameter of any point and the x-axis.

$$\begin{cases} x_2(\alpha') = r\cos\left(\dfrac{a\cot\alpha'+b}{r}\right) - \left(\dfrac{a}{\sin\alpha'}+r_\rho\right)\sin\left(\alpha' - \dfrac{a\cot\alpha'+b}{r}\right) \\ y_2(\alpha') = r\sin\left(\dfrac{a\cot\alpha'+b}{r}\right) - \left(\dfrac{a}{\sin\alpha'}+r_\rho\right)\cos\left(\alpha' - \dfrac{a\cot\alpha'+b}{r}\right) \end{cases} \tag{2}$$

Where r is the radius of the indexing circle, and the value range of the independent variable α' is $\alpha \le \alpha' \le \pi/2$;$a$, b and r_ρ represent tool parameters.

$$\begin{cases} x_3(\alpha_i) = r_i \sin\left(\dfrac{\pi}{2z} + inv\alpha - inv\alpha_i\right) \\ y_3(\alpha_i) = r_i \cos\left(\dfrac{\pi}{2z} + inv\alpha - inv\alpha_i\right) \end{cases} \tag{3}$$

Where r_i is the direction of any point on the involute; z is the number of teeth of the gear; α is the pressure angle of the indexing circle; α_i is the pressure angle at any position on the involute.

2.2. The meshing stiffness of gear was calculated by energy method

The potential energy of the gear tooth can be calculated by Timoshenko beam theory. The bending energy U_b, axial compressive energy U_a and shear energy U_s stored in a tooth can be calculated as

$$U_b = \frac{F^2}{2k_b},\ U_a = \frac{F^2}{2k_a},\ U_s = \frac{F^2}{2k_s} \tag{4}$$

The gear body is an important part connecting the shaft and the gear teeth. It is an elastic body collectively. When the gear teeth are loaded, the gear body will also bear the corresponding torque, resulting in the elastic deformation of the body. Based on Muskhelishvili theory, Sainsot and Velex regard the gear body with shaft holes as a deformable elastic ring, and propose a two-dimensional analytical formula to calculate the deformation of the gear body under load. In this paper, the finite element theory and the iron mosinker beam theory are used to divide the gear body into several elements, and then the energy method is used to calculate

ISSN: 2472-3703 DOI: 10.6911/WSRJ.202212_8(12).0020

the integral formula, so as to obtain the elastic deformation stiffness of the gear matrix. According to the finite element simulation results, the calculation results of this paper are obviously better than those of Sainsot and Velex.

As showen on Figure 1. When the number of fixed nodes in the gear shaft hole is n, the integral of the gear body can be divided into $n/2+1$ section. Assuming that the force of gear meshing is unit force, the formula for calculating the stiffness of gear body can be obtained according to Eq.(4), as shown in Eqs.(5)-(7).

$$U_{bf}=\frac{F^2}{2k_{bf}}=\sum_{i=1}^{n/2}\left(\int_{r_{in}\cdot\cos\left(\frac{2\pi}{n}\cdot\left(\frac{n}{2}-i+1\right)\right)}^{r_{in}\cdot\cos\left(\frac{2\pi}{n}\cdot\left(\frac{n}{2}-i\right)\right)}\frac{M_x{}^2(i)}{2EI_{1x}}dx\right)+\int_{r_{in}}^{x_C}\frac{M_x{}^2}{2EI_{1x}}dx \tag{5}$$

$$U_{af}=\frac{F^2}{2k_{af}}=\sum_{i=1}^{n/2}\left(\int_{r_{in}\cdot\cos\left(\frac{2\pi}{n}\cdot\left(\frac{n}{2}-i+1\right)\right)}^{r_{in}\cdot\cos\left(\frac{2\pi}{n}\cdot\left(\frac{n}{2}-i\right)\right)}\frac{F_x{}^2(i)}{2EA_{1x}}dx\right)+\int_{r_{in}}^{x_C}\frac{F_a{}^2}{2EA_{1x}}dx \tag{6}$$

$$U_{sf}=\frac{1}{2k_{sf}}=\sum_{i=1}^{n/2}\left(\int_{r_{in}\cdot\cos\left(\frac{2\pi}{n}\cdot\left(\frac{n}{2}-i+1\right)\right)}^{r_{in}\cdot\cos\left(\frac{2\pi}{n}\cdot\left(\frac{n}{2}-i\right)\right)}\frac{1.2F_y{}^2(i)}{2GA_{1x}}dx\right)+\int_{r_{in}}^{x_C}\frac{1.2F_b{}^2}{2GA_{1x}}dx \tag{7}$$

Where i is the integral on the i side; x_C represents the x-coordinate of the intersection of the dedendum transition curve and the dedendum circle, which are expressed as Eq.(8). A_{1x} represents the cross-sectional area at any point in the gear body, which are expressed as Eq.(9).

I_{1x} represents the moment of inertia of the section at any point in the gear body, which are expressed as Eq.(10).

$$x_C=r_f\cos(b/r) \tag{8}$$

$$A_{1x}=2\left(\sqrt{r_f^2-x_1^2}-\sqrt{r_f^2-\min\left(x_1^2,r_{in}^2\right)}\right)w \tag{9}$$

$$I_{1x}=\frac{2}{3}\left(\sqrt{r_f^2-x_1^2}^3-\sqrt{r_{in}^2-\min\left(x_1^2,r_{in}^2\right)}^3\right)w \tag{10}$$

In Eq.(5), $M_x(i)$ and M_x are the moment at the midpoint of any section, which are expressed as

$$M_x(i)=\sum_{n/2-i+2}^{n/2+i}\left(f_y(j)\left(x-r_{in}\cos\left(\left(\frac{2\pi}{n}\right)(j-1)\right)\right)+f_x(j)r_{in}\sin\left(\left(\frac{2\pi}{n}\right)(j-1)\right)\right) \tag{11}$$

$$M_x=F_a y_p-F_b\left(x_p-x\right) \tag{12}$$

In Eq.(6), $F_x(i)$ is the horizontal force used in the i^{th} integral, which are expressed as

ISSN: 2472-3703 DOI: 10.6911/WSRJ.202212_8(12).0020

$$F_x(i)=\sum_{n/2-i+2}^{n/2+i} f_x(j) \tag{13}$$

In Eq.(7), $F_y(i)$ is the vertical force used in the i^{th} integral, which are expressed as Eq.(14);G represent shear modulus, which are expressed as Eq.(15).

$$F_y(i)=\sum_{n/2-i+2}^{n/2+i} f_y(j) \tag{14}$$

$$G = E/\left[2(1+\mu)\right] \tag{15}$$

The total energy stored in the gear body is the sum of the three deformation energies, which can be expressed as

$$U_f = U_{af} + U_{bf} + U_{sf} \tag{16}$$

Where U_f represents the total energy of the gear fillet foundation.

According to the relationship between energy and stiffness, the stiffness of gear body can be expressed as

$$k_f = 1/\left(1/k_{bf} + 1/k_{af} + 1/k_{sf}\right) \tag{17}$$

Where k_f represents the fillet foundation stiffness of gear.

The deformation of tooth part is caused by meshing force, and the elastic deformation energy is formed by superposition of transition curve part and involute part of tooth root, and the calculation formula as

$$U_{bt} = \frac{F^2}{2k_{bt}} = \int_{x_C}^{x_B} \frac{M_x^2}{2EI_{2x}} dx_2 + \int_{x_B}^{x_P} \frac{M_x^2}{2EI_{3x}} dx_3 \tag{18}$$

$$U_{at} = \frac{F^2}{2k_{at}} = \int_{x_C}^{x_B} \frac{F_a^2}{2EA_{2x}} dx_2 + \int_{x_B}^{x_P} \frac{F_a^2}{2EA_{3x}} dx_3 \tag{19}$$

$$U_{st} = \frac{F^2}{2k_{st}} = \int_{x_C}^{x_B} \frac{1.2F_b^2}{2GA_{2x}} dx_2 + \int_{x_B}^{x_P} \frac{1.2F_b^2}{2GA_{3x}} dx_3 \tag{20}$$

Where A_{ix} represents the cross-sectional area of the tooth at any position, $A_{ix} = 2y_i w; I_{ix}$ is the moment of inertia between the tooth profile and the neutral surface of the tooth at any position,$I_{ix} = 2y_i^3 w/3; i = 2,3$ are the dedendum transition curve region and involute curve region respectively.

For the convenience of calculation, angular coordinates are adopted to represent each position, and the coordinates of the involute part can be expressed as

ISSN: 2472-3703 DOI: 10.6911/WSRJ.202212_8(12).0020

$$\begin{cases} x_3(\beta) = r_b\left((\beta_2+\beta)\sin\beta+\cos\beta\right) \\ y_3(\beta) = r_b\left((\beta_2+\beta)\cos\beta-\sin\beta\right) \end{cases} \tag{21}$$

Where β_2 is the base circle half,$\beta_2 = \pi/2z + \tan\alpha - \alpha$; β represents the angle between the meshing force and the vertical direction.

The derivative of the angles of Eqs.(21) and (2), respectively, can be expressed as

$$dx_3 = r_b(\beta_2+\beta)\cos\beta d\beta = f(\beta)d\beta \tag{22}$$

$$dx_2 = \begin{pmatrix} a\sin\left(\dfrac{a\cot\alpha'+b}{r}\right)\left(\cot^2\alpha'+1\right)+a\sin\left(\alpha'-\dfrac{a\cot\alpha'+b}{r}\right)\cdot\left(\dfrac{\cos\alpha'}{\sin^2\alpha'}\right)- \\ \cos\left(\alpha'-\dfrac{a\cot\alpha'+b}{r}\right)\left(\dfrac{a\left(\cot^2\alpha'+1\right)}{r}+1\right)\cdot\left(r_\rho+\dfrac{a}{\sin\alpha'}\right) \end{pmatrix} d\alpha' = g(\alpha')d\alpha' \tag{23}$$

Substituting Eqs.(22) and (23) into Eqs.(18)-(20), the bending ,axial compressive and shear stiffness are calculated as

$$\begin{aligned} \frac{1}{k_{bt}} = &\int_{\frac{\pi}{2}}^{\alpha}\frac{3\left[\cos\beta_P\left(x_P-x\right)-\sin\beta_P\cdot y_P\right]^2}{2E\omega y_{2x}^3}g(\alpha')d\alpha' \\ &+\int_{\beta_1}^{\beta_P}\frac{3\left[\cos\beta_P\left(x_P-x\right)-\sin\beta_P\cdot y_P\right]^2}{2E\omega y_{3x}^3}f(\beta)d\beta \end{aligned} \tag{24}$$

$$\frac{1}{k_{at}} = \int_{\frac{\pi}{2}}^{\alpha}\frac{\sin^2\beta_P}{2E\omega y_{2x}}g(\alpha')d\alpha' + \int_{\beta_1}^{\beta_P}\frac{\sin^2\beta_P}{2E\omega y_{3x}}f(\beta)d\beta \tag{25}$$

$$\frac{1}{k_{st}} = \int_{\frac{\pi}{2}}^{\alpha}\frac{1.2(1+\mu)\cos^2\beta_P}{E\omega y_{2x}}g(\alpha')d\alpha' + \int_{\beta_1}^{\beta_P}\frac{1.2(1+\mu)\cos^2\beta_P}{E\omega y_{3x}}f(\beta)d\beta \tag{26}$$

When the teeth are meshing, contact deformation exists between the two teeth at the meshing point, according to The Hertz contact theory, the contact deformation of two meshing gear teeth is regarded as two isotropic elastic cylinders contacting at the meshing point and deformed by extrusion. Yang and Sun used the first two terms of the square root binomial expansion to approximate the square root and calculate the Hertz deformation.It is verified that the accuracy of the results obtained by the approximate method is more than 99.5%.The Hertzian contact stiffness of the tooth surface can be calculated by

$$k_h = \frac{\pi E w}{4(1-\mu^2)} \tag{27}$$

Where E is the elastic modulus of tooth material;μ is the Poisson's ratio of tooth material;w is the contact width of the gear. According to Eq.(27), it can be obtained that the Hertzian contact stiffness is only related to the gear material and contact width. In spur gears, the gear contact

ISSN: 2472-3703 DOI: 10.6911/WSRJ.202212_8(12).0020

width is equal to the tooth width and remains constant during the meshing process, that is, the Hertzian contact stiffness is a constant value.

In order to ensure the continuity and smoothness of transmission motion of gear meshing, the contact degree of gear pair must be greater than 1, that is, the meshing process of gear pair is a process of single tooth and double tooth or even multiple pairs of teeth meshing alternately at the same time. Firstly, it is necessary to analyze the relationship between the meshing stiffness of a single pair of gear teeth and the stiffness of a single gear tooth.

When a single pair of gear teeth is loaded, the deformation energy is the sum of five kinds of deformation energy, which can be expressed as

$$U_m = U_h + U_{atp} + U_{btp} + U_{stp} + U_{fp} + U_{atg} + U_{btg} + U_{stg} + U_{fg} \tag{28}$$

Where, U_m is the total deformation energy;U_h is the Hertz contact deformation energy; a, b, s and f represent radial compression deformation, bending deformation, shear deformation and gear matrix deformation respectively; p and g represent pinion and gear respectively.

According to the relationship between stiffness and energy, the meshing stiffness of single tooth meshing gear pair can be expressed as

$$k_m = \frac{1}{\frac{1}{k_h} + \frac{1}{k_{atp}} + \frac{1}{k_{btp}} + \frac{1}{k_{stp}} + \frac{1}{k_{fp}} + \frac{1}{k_{atg}} + \frac{1}{k_{btg}} + \frac{1}{k_{stg}} + \frac{1}{k_{fg}}} \tag{29}$$

Where, k_m represents the comprehensive meshing stiffness in single tooth meshing.

In two-tooth meshing, two pairs of meshing teeth bear loads at the same time, which can be regarded as two pairs of teeth in series. The comprehensive meshing stiffness in two-tooth meshing can be expressed as

$$k_d = \frac{1}{\frac{1}{k_{m1}} + \frac{1}{k_{m1}}} = \frac{1}{\sum_{i=1}^{2} \frac{1}{\frac{1}{k_{hi}} + \frac{1}{k_{atpi}} + \frac{1}{k_{btpi}} + \frac{1}{k_{stpi}} + \frac{1}{k_{fpi}} + \frac{1}{k_{atgi}} + \frac{1}{k_{btgi}} + \frac{1}{k_{stgi}} + \frac{1}{k_{fgi}}}} \tag{30}$$

Where, k_d represents the comprehensive meshing stiffness in two-tooth meshing;$i = 1,2$ represent the first pair and the second pair respectively.

3. MESH STIFFNESS MODEL OF A CRACKED TOOTH

By studying the distribution of the maximum principal stress near the tooth root, Kramberger et al. found that when the Angle between the tangent line of the tooth root curve and the tooth centerline was 30°~34°, the tensile stress at the tangent point was the maximum.

ISSN: 2472-3703 DOI: 10.6911/WSRJ.202212_8(12).0020

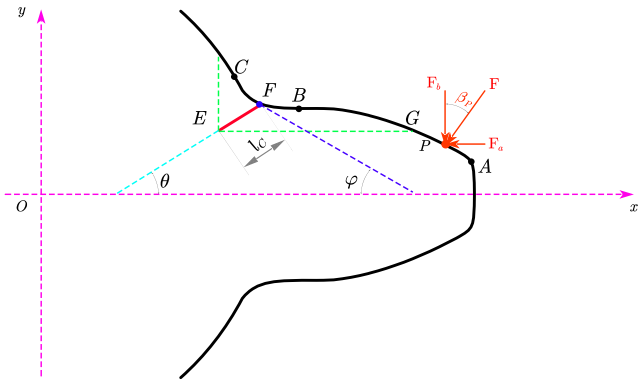

Figure 2. Model of a cracked tooth

As shown on Figure 2. Point F is the starting point of the crack; Point E is the termination point of the crack, which can be expressed as Eq.(31); l_C represents the length of the crack; θ represents the angle between the crack and the centerline of the gear tooth;

$$\begin{cases} x_E = x_F - l_c \cos(\theta) \\ y_E = y_F - l_c \sin(\theta) \end{cases} \tag{31}$$

3.1. The gear body stiffness

According to the position of the crack tip point, it can be divided into the following two cases:

Case1 When $x_E < x_C$

$$\frac{1}{k_{a1}} = \sum_{i=1}^{n/2} \left(\int_{r_{in}\cdot\cos\left(\frac{2\pi}{n}\cdot\left(\frac{n}{2}-i+1\right)\right)}^{r_{in}\cdot\cos\left(\frac{2\pi}{n}\cdot\left(\frac{n}{2}-i\right)\right)} \frac{F_x^{\,2}(i)}{EA_{1x1}} dx \right) + \int_{r_{in}}^{x_E} \frac{F_a^{\,2}}{EA_{1x1}} dx + \int_{x_E}^{x_C} \frac{F_a^{\,2}}{EA_{1x2}} dx \tag{32}$$

$$\frac{1}{k_{b1}} = \sum_{i=1}^{n/2} \left(\int_{r_{in}\cdot\cos\left(\frac{2\pi}{n}\cdot\left(\frac{n}{2}-i+1\right)\right)}^{r_{in}\cdot\cos\left(\frac{2\pi}{n}\cdot\left(\frac{n}{2}-i\right)\right)} \frac{M_x^{\,2}(i)}{EI_{1x1}} dx \right) + \int_{r_{in}}^{x_E} \frac{M_x^{\,2}(i)}{EI_{1x1}} dx + \int_{x_E}^{x_C} \frac{M_x^{\,2}(i)}{EI_{1x2}} dx \tag{33}$$

$$\frac{1}{k_{s1}} = \sum_{i=1}^{n/2} \left(\int_{r_{in}\cdot\cos\left(\frac{2\pi}{n}\cdot\left(\frac{n}{2}-i+1\right)\right)}^{r_{in}\cdot\cos\left(\frac{2\pi}{n}\cdot\left(\frac{n}{2}-i\right)\right)} \frac{1.2F_y^{\,2}(i)}{GA_{1x1}} dx \right) + \int_{r_{in}}^{x_E} \frac{1.2F_b^{\,2}}{GA_{1x1}} dx + \int_{x_E}^{x_C} \frac{1.2F_b^{\,2}}{GA_{1x2}} dx \tag{34}$$

Case2 When $x_E > x_C$

$$\frac{1}{k_{a1}} = \sum_{i=1}^{n/2} \left(\int_{r_{in}\cdot\cos\left(\frac{2\pi}{n}\cdot\left(\frac{n}{2}-i+1\right)\right)}^{r_{in}\cdot\cos\left(\frac{2\pi}{n}\cdot\left(\frac{n}{2}-i\right)\right)} \frac{F_x^{\,2}(i)}{EA_{1x1}} dx \right) + \int_{r_{in}}^{x_C} \frac{F_a^{\,2}}{EA_{1x1}} dx \tag{35}$$

$$\frac{1}{k_{b1}} = \sum_{i=1}^{n/2} \left(\int_{r_{in}\cdot\cos\left(\frac{2\pi}{n}\cdot\left(\frac{n}{2}-i+1\right)\right)}^{r_{in}\cdot\cos\left(\frac{2\pi}{n}\cdot\left(\frac{n}{2}-i\right)\right)} \frac{M_x^{\,2}(i)}{EI_{1x1}} dx \right) + \int_{r_{in}}^{x_C} \frac{M_x^{\,2}(i)}{EI_{1x1}} dx \tag{36}$$

ISSN: 2472-3703 DOI: 10.6911/WSRJ.202212_8(12).0020

$$\frac{1}{k_{s1}}=\sum_{i=1}^{n/2}\left(\int_{r_{in}\cdot\cos\left(\frac{2\pi}{n}\cdot\left(\frac{n}{2}-i\right)\right)}^{r_{in}\cdot\cos\left(\frac{2\pi}{n}\cdot\left(\frac{n}{2}-i+1\right)\right)}\frac{1.2F_y^{\,2}(i)}{GA_{1x1}}dx\right)+\int_{r_{in}}^{x_C}\frac{1.2F_b^{\,2}}{GA_{1x1}}dx \tag{37}$$

3.2. The stiffness of root transition curve part

According to the position of the crack tip point, it can be divided into the following four cases:

Case1 When $x_E < x_C$ and $y_E < y_B$

$$\frac{1}{k_{a2}}=\int_{x_C}^{x_B}\frac{\sin^2\beta_P}{EA_{2x2}}dx_2 \tag{38}$$

$$\frac{1}{k_{b2}}=\int_{x_C}^{x_B}\frac{\left[\cos\beta_P\left(x_P-x\right)-\sin\beta_P\cdot y_P\right]^2}{EI_{2x2}}dx_2 \tag{39}$$

$$\frac{1}{k_{s2}}=\int_{x_C}^{x_B}\frac{1.2(1+\mu)\cos^2\beta_P}{EA_{2x2}}dx_2 \tag{40}$$

Case2 When $x_E < x_C$ and $y_E > y_B$

$$\frac{1}{k_{a2}}=\int_{x_C}^{x_G}\frac{\sin^2\beta_P}{EA_{2x2}}dx_2+\int_{x_G}^{x_B}\frac{\sin^2\beta_P}{EA_{2x1}}dx_2 \tag{41}$$

$$\frac{1}{k_{b2}}=\int_{x_C}^{x_G}\frac{\left[\cos\beta_P\left(x_P-x\right)-\sin\beta_P\cdot y_P\right]^2}{EI_{2x2}}dx_2+\int_{x_G}^{x_B}\frac{\left[\cos\beta_P\left(x_P-x\right)-\sin\beta_P\cdot y_P\right]^2}{EI_{2x1}}dx_2 \tag{42}$$

$$\frac{1}{k_{s2}}=\int_{x_C}^{x_G}\frac{1.2(1+\mu)\cos^2\beta_P}{EA_{2x2}}dx_2+\int_{x_G}^{x_B}\frac{1.2(1+\mu)\cos^2\beta_P}{EA_{2x1}}dx_2 \tag{43}$$

Case3 When $x_E > x_C$ and $y_E < y_B$

$$\frac{1}{k_{a2}}=\int_{x_C}^{x_E}\frac{\sin^2\beta_P}{EA_{2x1}}dx_2+\int_{x_E}^{x_B}\frac{\sin^2\beta_P}{EA_{2x2}}dx_2 \tag{44}$$

$$\frac{1}{k_{b2}}=\int_{x_C}^{x_E}\frac{\left[\cos\beta_P\left(x_P-x\right)-\sin\beta_P\cdot y_P\right]^2}{EI_{2x1}}dx_2+\int_{x_E}^{x_B}\frac{\left[\cos\beta_P\left(x_P-x\right)-\sin\beta_P\cdot y_P\right]^2}{EI_{2x2}}dx_2 \tag{45}$$

$$\frac{1}{k_{s2}}=\int_{x_C}^{x_E}\frac{1.2(1+\mu)\cos^2\beta_P}{EA_{2x1}}dx_2+\int_{x_E}^{x_B}\frac{1.2(1+\mu)\cos^2\beta_P}{EA_{2x2}}dx_2 \tag{46}$$

Case4 When $x_E > x_C$ and $y_E > y_B$

ISSN: 2472-3703 DOI: 10.6911/WSRJ.202212_8(12).0020

$$\frac{1}{k_{a2}}=\int_{x_C}^{x_E}\frac{\sin^2\beta_P}{EA_{2x1}}dx_2+\int_{x_E}^{x_G}\frac{\sin^2\beta_P}{EA_{2x2}}dx_2+\int_{x_G}^{x_B}\frac{\sin^2\beta_P}{EA_{2x1}}dx_2 \tag{47}$$

$$\begin{aligned}\frac{1}{k_{b2}}=&\int_{x_C}^{x_E}\frac{\left[\cos\beta_P\left(x_P-x\right)-\sin\beta_P\cdot y_P\right]^2}{EI_{2x1}}dx_2+\int_{x_E}^{x_G}\frac{\left[\cos\beta_P\left(x_P-x\right)-\sin\beta_P\cdot y_P\right]^2}{EI_{2x2}}dx_2\\&+\int_{x_G}^{x_B}\frac{\left[\cos\beta_P\left(x_P-x\right)-\sin\beta_P\cdot y_P\right]^2}{EI_{2x1}}dx_2\end{aligned} \tag{48}$$

$$\frac{1}{k_{s2}}=\int_{x_C}^{x_E}\frac{1.2\left(1+\mu\right)\cos^2\beta_P}{EA_{2x1}}dx_2+\int_{x_E}^{x_G}\frac{1.2\left(1+\mu\right)\cos^2\beta_P}{EA_{2x2}}dx_2+\int_{x_G}^{x_B}\frac{1.2\left(1+\mu\right)\cos^2\beta_P}{EA_{2x1}}dx_2 \tag{49}$$

3.3. The stiffness of involute part

According to the position of the crack tip point, it can be divided into the following three cases:

Case1 When $y_E > y_B$

$$\frac{1}{k_{a3}}=\int_{x_B}^{x_P}\frac{\sin^2\beta_P}{EA_{3x1}}dx_3 \tag{50}$$

$$\frac{1}{k_{b3}}=\int_{x_B}^{x_P}\frac{\left[\cos\beta_P\left(x_P-x\right)-\sin\beta_P\cdot y_P\right]^2}{EI_{3x1}}dx_3 \tag{51}$$

$$\frac{1}{k_{s3}}=\int_{x_B}^{x_P}\frac{1.2\left(1+\mu\right)\cos^2\beta_P}{EA_{3x1}}dx_3 \tag{52}$$

Case2 When $y_A < y_E < y_B$,and $y_E > y_P$

$$\frac{1}{k_{a3}}=\int_{x_B}^{x_G}\frac{\sin^2\beta_P}{EA_{3x2}}dx_3+\int_{x_G}^{x_P}\frac{\sin^2\beta_P}{EA_{3x1}}dx_3 \tag{53}$$

$$\frac{1}{k_{b3}}=\int_{x_B}^{x_G}\frac{\left[\cos\beta_P\left(x_P-x\right)-\sin\beta_P\cdot y_P\right]^2}{EI_{3x2}}dx_3+\int_{x_G}^{x_P}\frac{\left[\cos\beta_P\left(x_P-x\right)-\sin\beta_P\cdot y_P\right]^2}{EI_{3x1}}dx_3 \tag{54}$$

$$\frac{1}{k_{s3}}=\int_{x_B}^{x_G}\frac{1.2\left(1+\mu\right)\cos^2\beta_P}{EA_{3x2}}dx_3+\int_{x_G}^{x_P}\frac{1.2\left(1+\mu\right)\cos^2\beta_P}{EA_{3x1}}dx_3 \tag{55}$$

Case3 When $y_E < y_A$ or ($y_A < y_E < y_B$ and $y_E < y_P$)

$$\frac{1}{k_{a3}}=\int_{x_B}^{x_P}\frac{\sin^2\beta_P}{EA_{3x2}}dx_3 \tag{56}$$

ISSN: 2472-3703 DOI: 10.6911/WSRJ.202212_8(12).0020

$$\frac{1}{k_{b3}}=\int_{x_B}^{x_P}\frac{\left[\cos\beta_P\left(x_P-x\right)-\sin\beta_P\cdot y_P\right]^2}{EI_{3x2}}dx_3 \tag{57}$$

$$\frac{1}{k_{s3}}=\int_{x_B}^{x_P}\frac{1.2\left(1+\mu\right)\cos^2\beta_P}{EA_{3x2}}dx_3 \tag{58}$$

In Eqs.(38)-(58). A_{ixj} is the cross-sectional area at any section, which can be expressed as Eq.(59); I_{ixj} is the moment of inertia at any section, which can be expressed as Eq.(60).

$$A_{ixj}=\begin{cases}2y_i\omega & j=1\\ \left(y_i+y_E\right)\omega & j=2\end{cases} \tag{59}$$

$$I_{ixj}=\begin{cases}\dfrac{2}{3}y_i^3\omega & j=1\\ \dfrac{1}{12}\left(y_i+y_E\right)^3\omega & j=2\end{cases} \tag{60}$$

4. STIFFNESS CALCULATION AND VERIFICATION

At present, the loaded tooth contact analysis method, analytical method, FEM and analytical-finite element method are the main calculation methods of the gear mesh stiffness, in which the calculation results of FEM are relatively accurate and widely used. Since other scholars have not studied the extension of tooth root crack to gear body, the feasibility of the proposed model is verified by FEM. The main parameters of spur gear pair are shown in Table 1, and the crack propagation angle, crack depth and percentage crack depth are presented in Table 2.

Table 1. Parameters of the gear dynamic model

Parameter	Pinion	Gear
Teeth number	23	31
Module (mm)	2.5	2.5
Teeth width (mm)	25	25
Pressure angle (°)	20	20
Poisson's ratio	0.3	0.3
Young modulus E (N/m^2)	$2.07\times\mathbf{10^{11}}$	$2.07\times\mathbf{10^{11}}$

Table 2. Crack parameters

Crack case	Crack propagation angle γ(°)	Crack depth l_c(mm)
#1	30	1.0
#2	30	1.8
#3	30	2.6

In order to verify the analytical model developed in this study, the mesh stiffness calculated by the finite element method (FEM) is used for comparison. Figure 5 displays the two-dimensional finite element model of a cracked pinion. In order to improve the calculation accuracy, the mesh around the contact region and the crack are refined. The radial

ISSN: 2472-3703 DOI: 10.6911/WSRJ.202212_8(12).0020

displacements of the inner ring nodes of the gear are constrained. According to the meshing process of the gear, the load is successively applied to the nodes on the involute from the tooth root to the tooth top, and the displacement of the meshing point is obtained. The stiffness of the gear at the meshing point is obtained according to $k = F/x$.

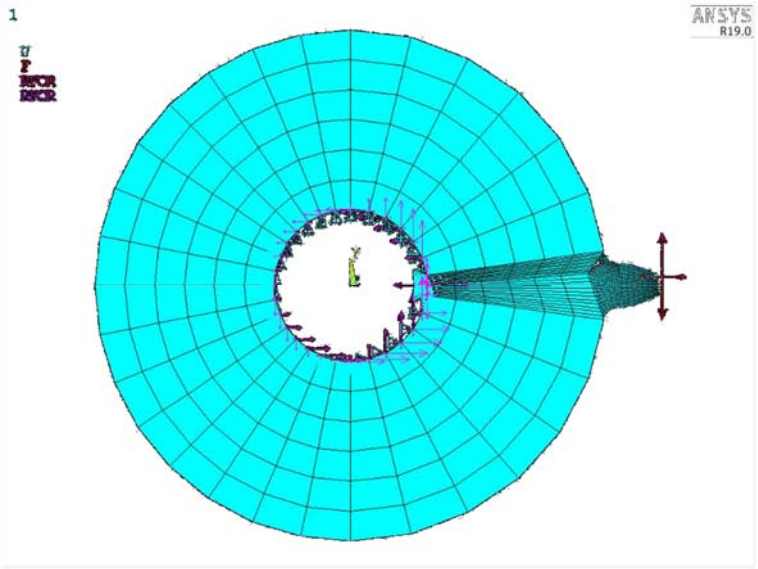

Figure 3. Two-dimensional FE model of the pinion with a crack

In the process of gear transmission, because the pinion bear higher speed and torque, so the crack often appears in the pinion.According to the data in Table 1 and Table **2**, the proposed method is compared with FEM, and the results are shown in Figure 4-Figure **6**.

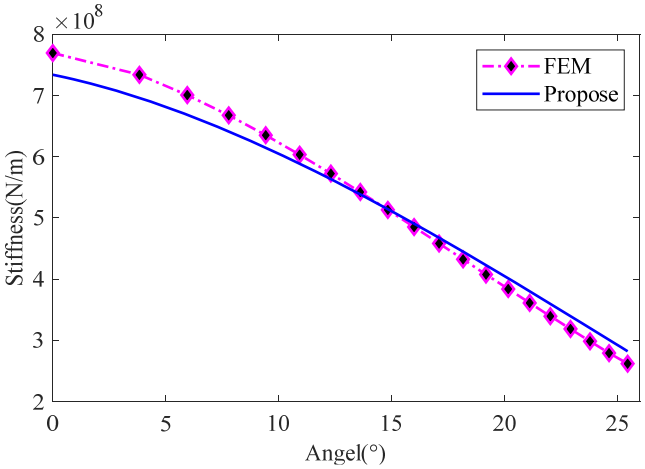

Figure 4. Comparison between the improved method and FEM with crack case #1

ISSN: 2472-3703 DOI: 10.6911/WSRJ.202212_8(12).0020

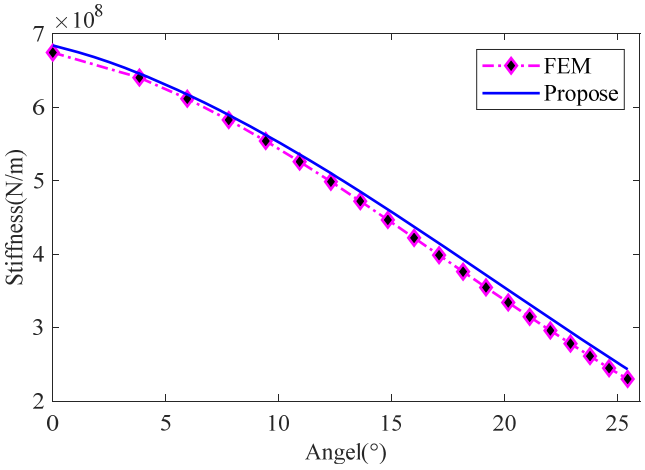

Figure 5. Comparison between the improved method and FEM with crack case #2

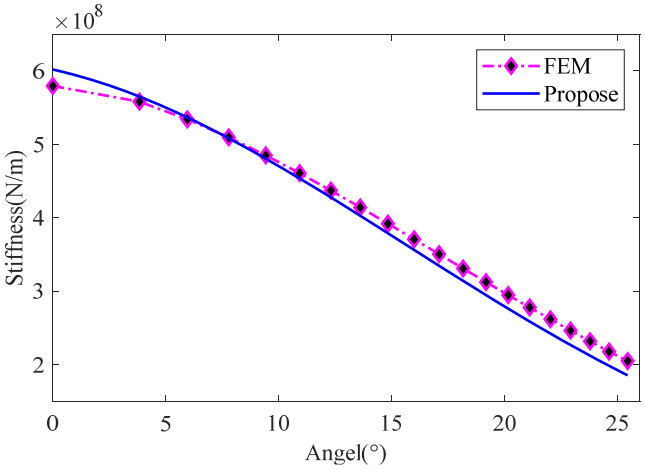

Figure 6. Comparison between the improved method and FEM with crack case #3

As can be seen from Figure 4-Figure **6**, the method proposed in this paper is very close to the FEM result, which also proves the feasibility of the method proposed in this paper.In order to more clearly see the influence of different crack depths on gear meshing stiffness, this paper presents Figure 7-Figure **8** according to the relationship of gear transmission.

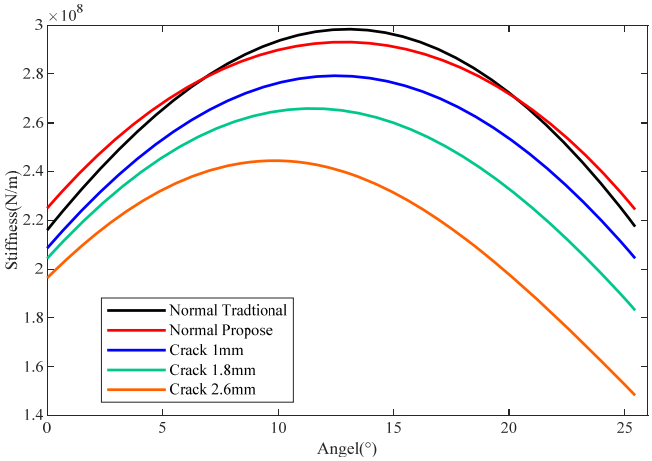

Figure 7. Comparison of single tooth meshing stiffness with different crack depths

ISSN: 2472-3703 DOI: 10.6911/WSRJ.202212_8(12).0020

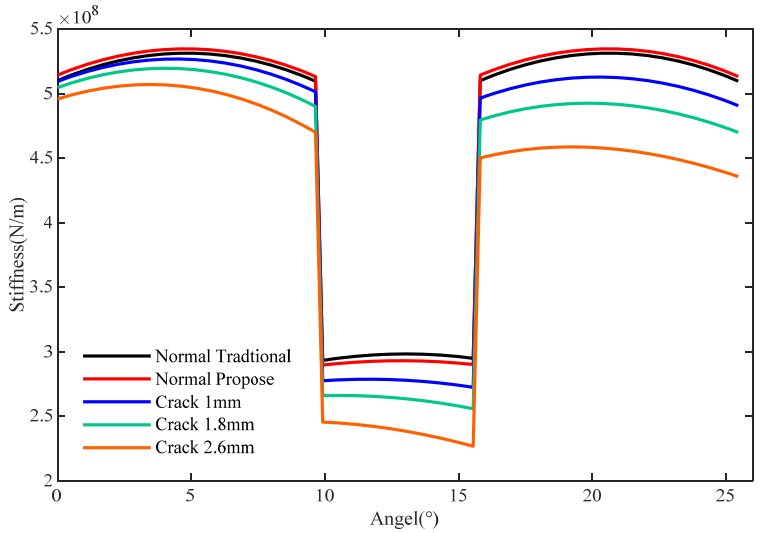

Figure 8. Comparison of comprehensive meshing stiffness at different crack depths

As can be seen from Figure 7-Figure **8**, with the increase of crack depth, both single tooth meshing stiffness and double tooth meshing stiffness decreased to different degrees, and the mutation was more drastic in the area where single and double teeth alternated.

5. CONCLUSION

In this paper, an analytical model of mesh stiffness of spur gears with crack extends into the gear body is presented. By comparing with FEM, the accuracy of the developed analysis method is verified, and the effect of crack length is analyzed. The proposed analytical model can provide relatively accurate mesh stiffness for spur gear with cracks by considering the deformation of the gear body. The presence of cracks makes the mesh stiffness of crack teeth decrease during the complete rotation. The mesh stiffness of crack teeth decreases with the increase of crack length.

REFERENCES

[1] Weber C: The deformation of loaded gears and the effect on their load-carrying capacity[J], Sponsored Research (Germany), British Dept of Scientific and Industrial Research, Report, (1949) No.3.

[2] Cornell R: Compliance and stress sensitivity of spur gear teeth[J], (1981).

[3] Yang D, Lin J: Hertzian damping, tooth friction and bending elasticity in gear impact dynamics[J], (1987).

[4] Tian X: Dynamic simulation for system response of gearbox including localized gear faults[J], (2004).

[5] Sainsot and P, Velex P: Duverger O. Contribution of gear body to tooth deflections—a new bidimensional analytical formula[J], Vol. 126 (2004) No. 4, P. 748-752.

[6] Chen Z., Shao Y: Dynamic simulation of spur gear with tooth root crack propagating along tooth width and crack depth[J], Engineering Failure Analysis, Vol. 18 (2011) No. 8, P. 2149-2164.

[7] Wang J: Numerical and experimental analysis of spur gears in mesh[D], Curtin University, (2003).

[8] Chaari F, Baccar W, Abbes M.S: Effect of spalling or tooth breakage on gearmesh stiffness and dynamic response of a one-stage spur gear transmission[J], European Journal of Mechanics-A/Solids, Vol. 27 (2008) No. 4, P. 691-705.

[9] Pandya Y, Parey A: Failure path based modified gear mesh stiffness for spur gear pair with tooth root crack[J], Engineering Failure Analysis, Vol. 27 (2013) No. 3, P. 286-296.

ISSN: 2472-3703 DOI: 10.6911/WSRJ.202212_8(12).0020

[10] Wan Z, Cao H, Zi Y: An improved time-varying mesh stiffness algorithm and dynamic modeling of gear-rotor system with tooth root crack[J], Engineering Failure Analysis, Vol. 42 (2014) No. 3, P. 157-177.

[11] Ma H, Pang ., Feng R: Improved time-varying mesh stiffness model of cracked spur gears[J], Engineering Failure Analysis, Vol. 55 (2015) P. 271-287.

[12] Chen Y, Jin Y, Liang X: Propagation path and failure behavior analysis of cracked gears under different initial angles[J], Mechanical Systems and Signal Processing, Vol. 110 (2018) P. 90-109.

[13] Liang X, Zuo M: Pandey M. Analytically evaluating the influence of crack on the mesh stiffness of a planetary gear set[J], Mechanism and Machine Theory, Vol. 76 (2014) P. 20-38.